Estimation Earthquake Source Parameters in Mentawai Island Region Using Moment Tensor

Fahmia Zuwidhatul Husna*,[1] Sungkono,[1] Muhammad Nurul Fahmi,[2] Eko Minarto,[1] and Saifuddin[1]

[1]*Department of Physics, Institut Teknologi Sepuluh Nopember, Surabaya 60111*
[2]*Department of Physics, Universitas Negeri Surabaya, Surabaya 60231*

Abstract: The Mentawai Islands is a seismically active zone that often experiences earthquakes due to the interaction of tectonic plates, so it is necessary to analyze the earthquake source parameters to understand its characteristics. This study aimed to determine earthquake source parameters for events of M_w $\geq$ 5.5 that occurred in 2023 using moment tensor inversion. Three-component waveform data from the GEOFON network were analyzed in the time domain, filtered within a frequency range of 0.01 to 0.025 Hz. The inversion yielded variance reduction (VR) values above 70% (88.24%, 81.98%, 94.05%, and 73.16%), indicating a good fit between observed and synthetic waveforms. The results of waveform data analysis show that the earthquake in the study area was caused by tectonic activity characterized by the percentage of Double-Couple (DC) more dominant than Compensated Linear Vector Dipole (CLVD), at shallow depths. Comparison with earthquake catalogs (GCMT, USGS, and GFZ) showed agreement, supported by Kagan angle values below 60°. In addition, the focal mechanism of the waveform data analysis indicated that the type of fault that causes the earthquake in the study area was a reverse fault.

Keywords: Moment tensor; Earthquake; Mentawai; MTtime

*Corresponding author: fahmiazhusna@outlook.com

http://dx.doi.org/10.12962/j24604682.v21i3.22563
2460-4682

I. INTRODUCTION

The Mentawai Islands are near the Sumatra subduction zone, formed by the impact of the Indo-Australian Plate that plunged down the Eurasian Plate [1]. The convergence of the two plates caused the Mentawai Islands area have high seismic activity. One of the earthquakes around the Mentawai Islands was an earthquake with a magnitude of M_w 7.8 that resulted in a devastating tsunami in 2010 [2-5].

Given the frequent seismic events in this region, moment tensor analysis becomes essential to characterize the earthquake source mechanisms accurately. Through moment tensor calculations, we can better understand seismic sources occuring in this tectonically activity area. Thus, this research aimed to determine the earthquake sources parameters using tensor moment inversion in the Mentawai Islands area. Determination of earthquake source parameters provides information related to earthquake source mechanisms, which is useful for seismic hazard assessment, plate movement, fault characterization, and regional tension fields [6]. Tensor moment inversions can be used to determine the source mechanism of earthquakes. This process requires that the synthetic seismogram be represented as a linear combination of fundamental Green's functions, with the weights on the Green's functions being individual moment tensor elements. [7].

Understanding the characteristics of earthquake sources is essential for assessing seismic hazards, especially in tectonically active regions such as the Mentawai Islands. Although many previous studies have analyzed large subduction earthquakes in this region, detailed source mechanism studies using moment tensor inversion for moderate events remain limited. This study addresses this gap by applying time-domain moment tensor inversion to multiple moderate to large earthquakes.

This study integrated waveform inversion and moment tensor decomposition to analyze both the geometric properties of faulting expressed through strike, dip, rake, and the compositional characteristics of the seismic source, including double couple, isotropic, and compensated linear vector dipole components. A detailed examination of these parameters provides a deeper understanding of the faulting processes and offers new perspectives on the tectonic behavior along the Mentawai segment. The results may enhance interpretations of seismotectonic activity and improve the reliability of seismic hazards in subduction zone environments.

II. METHODOLOGY

This study applies moment tensor inversion to estimate earthquake source parameters representing the physical characteristics of faulting processes. The estimated parameters include the six components of the moment tensor, moment magnitude (M_w) and the orientation of the focal mechanism expressed through the fault plane solution (strike, dip, and rake). In addition, the inversion results were further analyzed based on their constituent components double couple (DC), isotropic (ISO), and compensated linear vector dipole (CLVD), to assess the dominant type of seismic source involved.

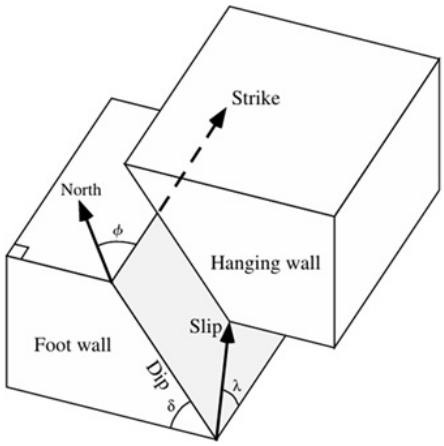

FIG. 1: The fault plane defined by the strike and dip of the fault surface and the direction of the slip vector [11].

TABLE I: Mentawai Islands earthquake event data 2023 $M_w \geq 5.5$.

No	Date (UTC)	Lat	Long	M_w	Depth (km)
1	2023-04-22 17:09:45	-0.77	98.58	5.8	26.714
2	2023-04-22 21:17:47	-0.94	95.49	5.7	20
3	2023-04-24 20:00:57	-0.80	98.52	7.1	34
4	2023-06-20 08:39:17	-0.97	98.61	5.5	19.709

The seismic tensor moment is a 3 × 3 matrix that is symmetrical [8], due to its symmetrical nature (M_{12} = M_{21}, M_{13} = M_{31}, and M_{23} = MM_{32}), only its six components are independent. The components of the tensor moment are M_{11}, M_{12}, M_{13}, M_{22}, M_{23}, dan M_{33}. The six components of a tensor moment can be separated into three eigenvalues (Eq. (1)) that characterize magnitude, a tensor moment "source type" and three angles (strike, dip, and rake) that provide the orientation of the tensor moment [9-10].

$$\mathbf{M} = M_1 e_1 \otimes e_1 + M_2 e_2 \otimes e_2 + M_3 e_3 \otimes e_3 \qquad (1)$$

The determination of the focal mechanism can be efficiently obtained through grid search computation based on three parameters that determine the focal mechanism (strike, dip, rake). Strike, dip, and rake/slip angle are three angles that describe the orientation of the fault plane and the direction of block movement during an earthquake (Fig. 1) [11]. Strike

TABLE II: Mentawai Islands earthquake recording station 2023 $M_w \geq 5.5$.

No	Network	Station	Lat	Long	Channel	Component
1	GE	GSI	1.3039	97.5755	BH	ZRT
2	GE	MNAI	-4.3605	102.9554	BH	ZRT
3	GE	LHMI	5.2288	96.9472	BH	ZRT
4	GE	PMBI	-2.9024	104.6993	BH	ZRT

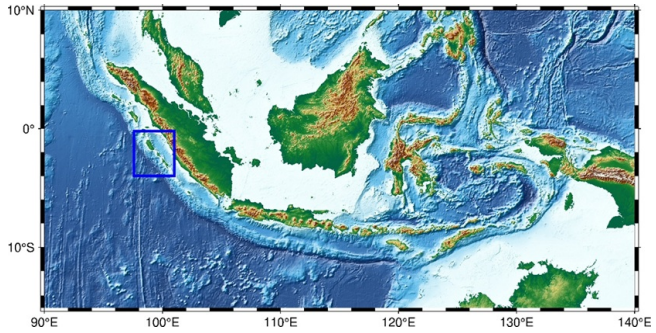

FIG. 2: Research Location, Mentawai Islands in a blue box.

($0 \leq \phi \leq 360°$) is the angle between the north direction and the horizontal line in the fault plane measured clockwise. Dip ($0 \leq \delta \leq 90°$) is the angle of inclination of the fault plane to the horizontal plane. Rake/slip ($0 \leq \lambda \leq 360°$) is the angle that indicating the direction of movement of the fault block relative to the fault plane, as measured from the strike line.

The three components of Eq. (1) can be rearranged into the three main components of Eq. (2), which are Isotropic (ISO), Double-Couple (DC), dan Compensated Linear Vector Dipole (CLVD) [12-14].

$$\begin{aligned} \mathbf{M} &= \mathbf{M}_{ISO} + \mathbf{M}_{DC} + \mathbf{M}_{CLVD} \\ &= M_{ISO}\mathbf{E}_{ISO} + M_{DC}\mathbf{E}_{DC} + M_{CLVD}\mathbf{E}_{CLVD} \end{aligned} \qquad (2)$$

$\mathbf{E}_{ISO}$, $\mathbf{E}_{DC}$, dan $\mathbf{E}_{CLVD}$ sequentially indicate the basic tensor ISO, DC, dan CLVD, while M_{ISO}, M_{DC}, M_{CLVD} sequentially are moments ISO, DC, dan CLVD. Generally, the tensor moment of a double couple (DC) representation of the force due to the shift of two blocks along the fault, which is dominant in earthquakes caused by tectonic earthquakes [6], [9], [15]. Meanwhile, non-double couple components (CLVD and ISO) usually describe earthquakes that cannot be fully explained by shear shifts in the fault plane, for example due to explosions [16, 17], mining activities [18-20], and earthquakes due to volcanic activity [21, 22].

To better understand these seismic source mechanisms in a world context, we analyzed seismic events in the Mentawai Island region (Fig. 2). This area was chosen due to its significant tectonic activity. Three-component waveform data ware selected based on the criteria for an earthquake that occurred in the Mentawai Islands area in 2023 with a moment magnitude $M_w \geq 5.5$. Waveform data is obtained automatically using ObsPy [23] through the Incorporated Research Institutions for Seismology (IRIS) data center with a network of GE stations. The data were corrected by the instrument's response to ground motion [24], rotated from ZNE to ZRT [24, 25], and filtered by bandpass filtering [26]. Bandpass filters were also applied to synthetic data calculations.

Earthquake data are presented in Table I, and recording station used in this study are presented in Table II. The visualization between the four earthquake sources and the earthquake receiving station is depicted in Fig. 3.

Fig. 3 shows both earthquake and station locations in the Mentawai Islands area in 2023 with magnitude $M_w \geq 5.5$.

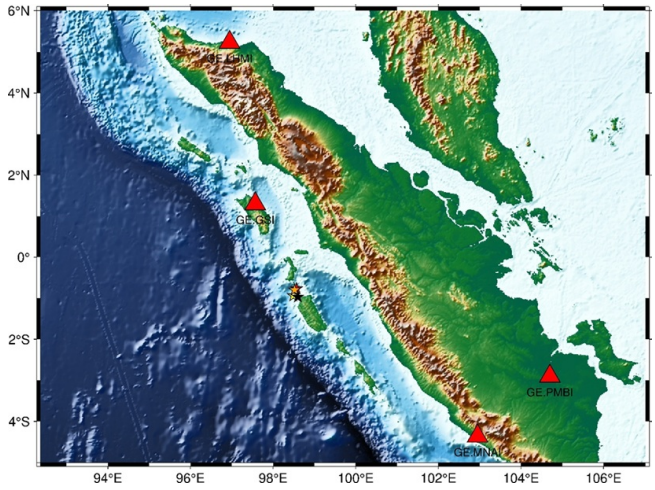

FIG. 3: Earthquake location (star) and seismic station recording (red triangle) of the 2023 $M_w \geq 5.5$ Mentawai Islands earthquake; event red star symbols 20230422_170945, yellow 20230422_211747, orange 20230424_200057, and black for event 20230620_083917.

Four earthquake events occur at time and magnitude as per Table I, and recorded by the same four stations, GE.GSI, GE.MNAI, GE.LHMI, and GE.PMBI.

Green functions synthetic data calculated based on the frequency-wavenumber integration method using Computer Programs in Seismology (CPS) software [27]. The Green function describes how the earth responds to the impulse of the point force applied to its source, representing seismic waves propagation from source to recording station. The weight of the Green function is the element of the individual tensor moment [6, 11]. In order to obtain good calculation results, the selection of an appropriate earth model is very influential. In this study, a 1-D GIL7 earth model was used [28].

The data were inverted to obtain tensor moment solution. Inversion of the tensor moment performed in time domain for each recorded earthquake event. Earthquake data in the form of a three-component waveform were processed to estimate the following source parameters: source depth, focal mechanism, and total seismic moment. MTtime [29] used as software to run inversions based on least-square generalized inversions [7]. The fitness between observation and synthetic data was measured by reduction variant (VR) [30]:

$$VR = \left[1 - \frac{\Sigma_i \left(d_i - s_i\right)^2}{\Sigma_i d_i^2}\right] \times 100 \qquad (3)$$

By d_i being observational data, and s_i being synthetic data.

III. RESULTS AND DISCUSSION

Calculation of tensor moment inversion was carried out using depth variation of 20 km to 40 km with interval of 1 km. Each earthquake in this study is MW 5.8, 5.7, 7.1, and 5.5, so the appropriate frequency to be used is in the range 0.01-0.05 Hz [31]. The inversion results for each earthquake were calculated by Kagan angle [32] to determine the suitability of the research with earthquake catalogs. The calculation of Kagan angle uses comparison between parameters of the fault plane (strike, dip, rake) of the study and the earthquake catalog. The earthquake catalog used for comparison was from GCMT (https://www.globalcmt.org/CMTsearch.html) [33], USGS (https://earthquake.usgs.gov/earthquakes/search) [34], and GFZ [35]. The result is said to be appropriate if the calculation result are obtained $< 60°$ [36-38].

TABLE III: Comparison of event 20230422_170945 inversion results with earthquake catalog.

Parameter	This Study	GCMT	USGS	GFZ
Beachball				
M_w	6.16	6	5.78	5.76
Depth (Km)	20	20	35.5	26
Strike1 (°)	138	129	136	140
Dip1 (°)	77	78	63	51
Rake1 (°)	88	84	76	88
Strike2 (°)	327	335	345	323
Dip2 (°)	14	13	30	39
Rake2 (°)	98	115	115	93
Fault Type	Reverse	Reverse	Reverse	Reverse
Kagan Angle (°)		9.46	17.18	25.08

1. Event 20230422_170945
   The tensor moment solution for 20230422_170945 earthquake is presented in Fig. 4. The frequency filter range used is 0.01-0.02 Hz. The compatibility between observation and synthetic data was demonstrated by high variance reduction (VR) value of 88.24%. The percentage of double-couple (DC) components is also more dominant over compensated linear vector dipole (CLVD) component, that the earthquake occur due to tectonic earthquake.

   Comparison of research results with earthquake cata-

TABLE IV: Comparison of event 20230422_211747 inversion results with earthquake catalog.

Parameter	This Study	GCMT	USGS	GFZ
Beachball				
M_w	5.93	5.9	5.67	5.8
Depth (Km)	31	24.1	17.5	22
Strike1 (°)	127	133	139	126
Dip1 (°)	66	72	63	75
Rake1 (°)	91	87	89	78
Strike2 (°)	304	324	320	345
Dip2 (°)	24	18	27	19
Rake2 (°)	87	101	91	127
Fault Type	Reverse	Reverse	Reverse	Reverse
Kagan Angle (°)		10.25	13.32	15.55

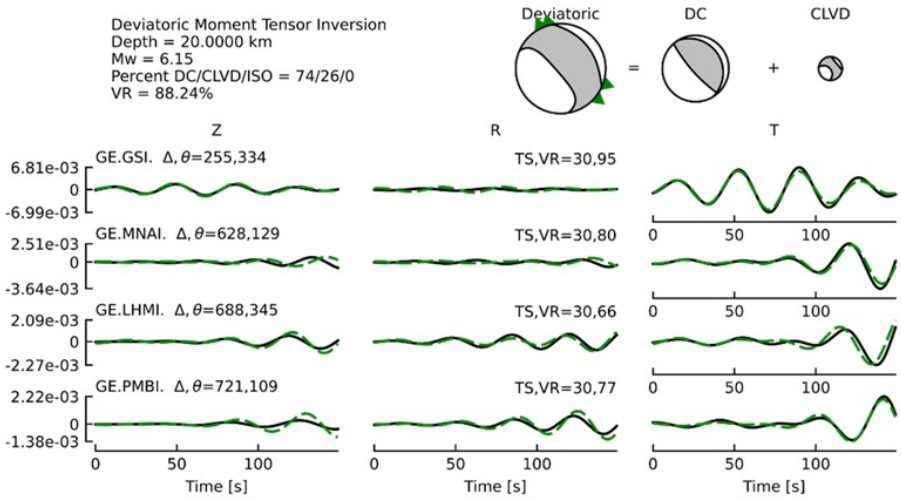

FIG. 4: Inversion result event 20230422_170945.

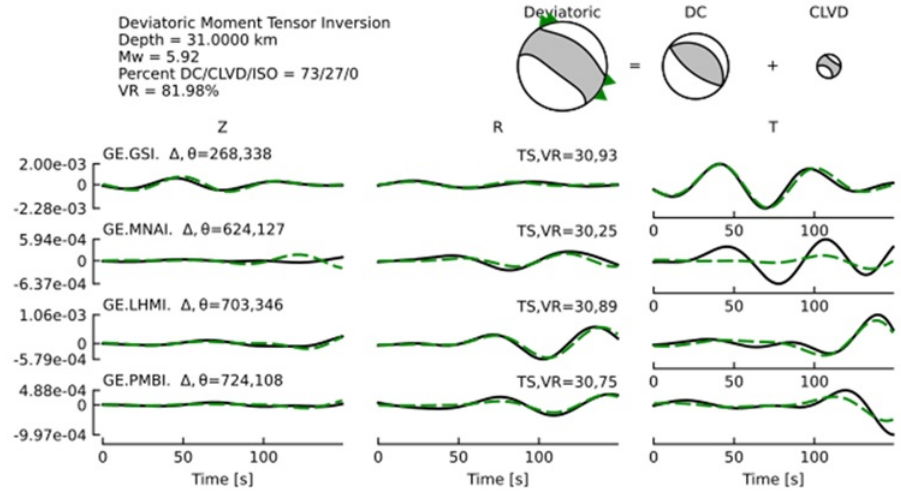

FIG. 5: Inversion result event 20230422_211747.

logs is presented in Table III. Beachball result shows that an earthquake was occur caused by reverse fault. Kagan angle calculation showed a good fitness between the data of this study and earthquake catalogs (GCMT, USGS, GFZ).

2. Event 20230422_211747
The inversion results for the 20230422_211747 event shown in Fig. 5. The frequency range used was 0.01-0.02 Hz for the filtering stage, which produced a VR value of 81.98%. The VR value was relatively high; thus, it can be said that the inversion results are good. The best solution for the inversion result is at a depth of 31 km with a magnitude Mw 5.92. Additionally, the DC component is valued at 73%, larger than the CLVD component which is valued at 27%. The dominant DC component indicates that the earthquake occurred due to a tectonic earthquake.

Table IV presents the results of the study compared with centroid results from various sources, such as GCMT, USGS, and GFZ. The results of the beachball representation in this study and the earthquake catalogs show the type is reverse fault. The calculation of the Kagan angle is carried out by comparing strike, dip, and rake values from 2 sources. The results of the Kagan angle calculation of this study with GCMT showed a value of 10.25°, with USGS 13.32°, and with GFZ 15.55° which indicates that the results of this study are in accordance with the results of earthquake catalogs.

3. Event 20230424_200057
The 20230424_200057 event was the largest earthquake in this study. Based on Fig. 6, the best solution for inversion was at a depth of 20 km with a magnitude of M_w 7.06. The inversion process that has been carried out shows excellent results judging from the very high VR

TABLE V: Comparison of event 20230424_200057 inversion results with earthquake catalog.

Parameter	This Study	GCMT	USGS	GFZ
Beachball				
M_w	7.06	7	7.12	6.87
Depth (Km)	20	27.5	17.5	20
Strike1 (°)	135	128	133	129
Dip1 (°)	78	76	83	74
Rake1 (°)	89	86	90	85
Strike2 (°)	321	322	313	328
Dip2 (°)	12	15	7	17
Rake2 (°)	96	104	90	108
Fault Type	Reverse	Reverse	Reverse	Reverse
Kagan Angle (°)		7.2481	5.53	7.50

TABLE VI: Comparison of event 20230620_083917 inversion results with earthquake catalog.

Parameter	This Study	GCMT	USGS	GFZ
Beachball				
M_w	5.78	5.7	5.49	5.58
Depth (Km)	20	22	21.5	25
Strike1 (°)	128	130	131	134
Dip1 (°)	56	76	71	76
Rake1 (°)	74	85	79	86
Strike2 (°)	336	333	342	329
Dip2 (°)	37	15	22	15
Rake2 (°)	113	112	119	104
Fault Type	Reverse	Reverse	Reverse	Reverse
Kagan Angle (°)		22.49	15.66	22.78

value, which is 94.05%. The earthquake source mechanism is dominated by DC components by 94%, with the contribution of CLVD being only 6%. This indicates that the earthquake was almost purely caused by fault movement. The filter used in this study was 0.01-0.02 Hz.

Table V shows the beachball representation of this study for the 20230422_211747 event is a type of reverse fault, as well as from GCMT, USGS, and GFZ are also types of reverse faults. For the strike, dip, and rake values in the study compared to the earthquake catalogs using the Kagan angle as before, the results of small Kagan angles (7.2481°, 5.53°, and 7.50°) were obtained, which showed the conformity of the calculation of the inversion results of this study with GCMT, USGS, and GFZ.

4. Event 20230620_083917
The results of the inversion are shown in Fig. 7, where the best solution was obtained at a depth of 20 km with a magnitude M_w 5.77. The DC component is valued at 54%, slightly larger than the CLVD component which is 46%. The quality of the inversion results can still be said to be quite good with a VR score of 73.16%. Although this value is the smallest of the 3 previous earthquakes, the wave recordings from the four stations (GE. GSI, GE. MNAI, GE. LHMI, and GE. PMBI) still shows a fairly good match between observation data and synthetic data. The filter used in this study was 0.015-0.025 Hz.

Comparison of research results with earthquake catalogs is presented in Table VI. The results of the beachball representation show that the type of fault is reverse fault. The calculation of the Kagan value in the 20230620_083917 event still showed a good match (the calculation result is less than 60°). Each of the Kagan values in this study was 22.49°, 15.66°, and 22.78°.

Based on the data presented in Table VII, the moment tensor components for each earthquake event exhibit a high degree of consistency. The uniform pattern of

TABLE VII: Moment tensor components for the 2023 Mentawai Islands earthquake $M_w \geq 5.5$.

Moment tensor component	Earthquake event 20230422_170945	20230422_211747	20230424_200057	20230620_083917
Mrr	7,905e+24	5,291e+24	1,638e+26	3,384e+24
Mtt	-1,361e+24	-4,070e+24	-7,100e+25	-1,158e+24
Mpp	-3,803e+24	-1,646e+24	-9,082e+25	-2,452e+24
Mrt	1,043e+25	4,169e+24	2,760e+26	1,438e+24
Mrp	-1,169e+25	-3,242e+24	-2,774e+26	-7,693e+23
Mtp	5,185e+24	3,736e+24	9,411e+25	3,035e+24

tensor components across events indicates similarity in the source mechanisms within the study area. Specifically, the Mrr component shows positive values for all analyzed events, which physically represent upward vertical motion during the seismic deformation process [39]. The positive Mrr values suggest that the dominant fault mechanism is a reverse fault, which is commonly associated with active subduction zones such as the Mentawai Islands region.

Based on the inversion result that has been carried out for each earthquake event in this study, all beachballs represent reverse fault. This result is well-suited by previous research that dominant type of fault that occurs in the Mentawai Islands area is reverse fault [40, 41], although other studies have declared that the Mentawai Islands fault is a strike-slip fault [42]. Each earthquake event in this study is located in the Mentawai Islands segment. Fig. 8 shows a visualization of the beachball and station locations that recorded the four earthquake events in this study.

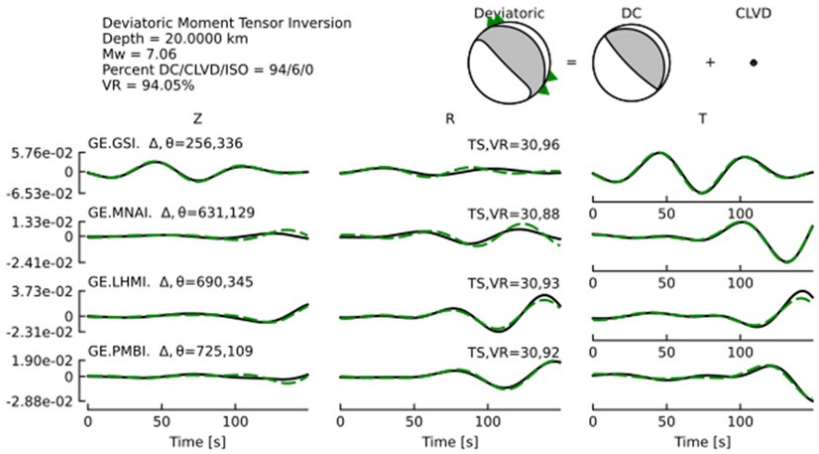

FIG. 6: Inversion result event 20230424_200057.

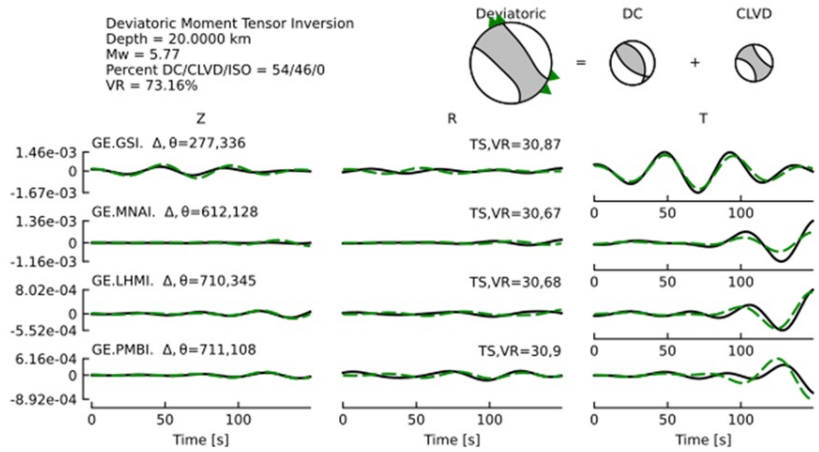

FIG. 7: Inversion result event 20230620_083917.

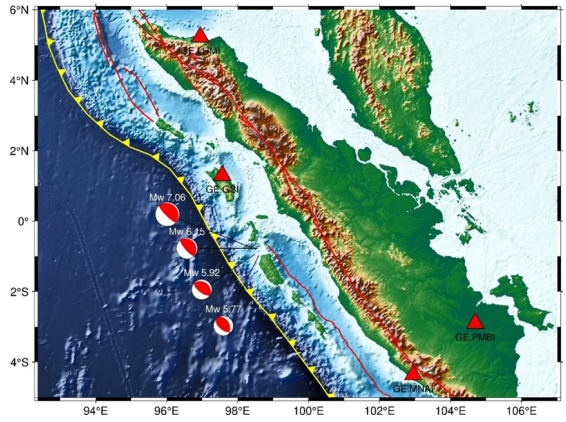

FIG. 8: Representation of beachball and earthquake recording station of Mentawai Islands 2023 Mw $\geq$ 5.5.

IV. CONCLUSION

The determination of the earthquake source was successfully carried out by moment tensor inversion, as evidenced by the high varian reduction (VR) values for all events (88.24%, 81.98%, 94.05%, and 73.16%). The resulting source mechanisms also presented a good fitness with established earthquake catalogs, including GCMT, USGS, and GFZ based on Kagan angle values, all of which were below 60° (Kagan angles value for the first earthquake 9.46°, 17.18°, and 25.08°; the second event 10.25°, 13.32°, and 15.55°; the third event 7.25°, 5.53°, and 7.50°; and the fourth event 22.49°, 15.66°, and 22.78°).

Acknowledgments

We would like to thank Andrea Chiang and Lawrence Livermore National Laboratory (LLNL) for invaluable contribution to the development of the MTtime software, which used

in this study. The visualization of the research area (Fig. 1), earthquake and stations locations (Fig. 3), and beachball representations (Fig. 8) were visualized using pyGMT [43].

[1] F.Z. Shabrina, *et al.*, "Measure coastal disaster resilience using community disaster resilience index (CDRI) in Mentawai Island, Indonesia," AIP Conference Proceedings, vol. 1987, no. 1, p. 020080, Jul. 2018, doi: 10.1063/1.5047365.

[2] T. Lay, *et al.*, "The 25 October 2010 Mentawai tsunami earthquake (Mw 7.8) and the tsunami hazard presented by shallow megathrust ruptures: OCTOBER 2010 MENTAWAI TSUNAMI EARTHQUAKE," Geophys. Res. Lett., vol. 38, no. 6, p. n/a-n/a, Mar. 2011, doi: 10.1029/2010GL046552.

[3] E.M. Hill, *et al.*, "The 2010 Mw 7.8 Mentawai earthquake: Very shallow source of a rare tsunami earthquake determined from tsunami field survey and nearfield GPS data," J. Geophys. Res., vol. 117, no. B6, p. 2012JB009159, Jun. 2012, doi: 10.1029/2012JB009159.

[4] L. Zhang, *et al.*, "Estimation of the 2010 Mentawai tsunami earthquake rupture process from joint inversion of teleseismic and strong ground motion data," Geodesy and Geodynamics, vol. 6, no. 3, p. 180-186, May 2015, doi: 10.1016/j.geog.2015.03.005.

[5] A.V. Newman, *et al.*, "The 25 October 2010 Mentawai tsunami earthquake, from real-time discriminants, finite-fault rupture, and tsunami excitation," Geophysical Research Letters, vol. 38, no. 5, Mar. 2011, doi: 10.1029/2010GL046498.

[6] A. Chiang, *et al.*, "Seismic source characterization of the Arabian Peninsula and Zagros Mountains from regional moment tensor and coda envelopes," Arab J Geosci, vol. 14, no. 1, p. 9, Jan. 2021, doi: 10.1007/s12517-020-06266-x.

[7] S.E. Minson, and D.S. Dreger, "Stable inversions for complete moment tensors," Geophysical Journal International, vol. 174, no. 2, p. 585-592, Aug. 2008, doi: 10.1111/j.1365-246X.2008.03797.x.

[8] T. Lay, and T.C. Wallace, "Modern global seismology", in International geophysics series, no. v. 58. San Diego: Academic Press, 1995.

[9] C. Alvizuri, *et al.*, "Estimation of full moment tensors, including uncertainties, for nuclear explosions, volcanic events, and earthquakes," Journal of Geophysical Research: Solid Earth, vol. 123, no. 6, p. 5099-5119, 2018.

[10] V. Vavryuk, "Moment Tensors: Decomposition and Visualization," in Encyclopedia of Earthquake Engineering, M. Beer, I. A. Kougioumtzoglou, E. Patelli, and I. S.-K. Au, Eds., Berlin, Heidelberg: Springer Berlin Heidelberg, 2015, p. 1-16. doi: 10.1007/978-3-642-36197-5_288-1.

[11] P.M. Shearer, "INTRODUCTION TO Seismology", SECOND EDITION. New York: Cambridge University Press, 2009. [Online]. Available: www.cambridge.org/9780521882101

[12] T.J. Fitch, D.W. McCowan, and M.W. Shields, "Estimation of the seismic moment tensor from teleseismic body wave data with applications to intraplate and mantle earthquakes," Journal of Geophysical Research: Solid Earth, vol. 85, no. B7, p. 3817-3828, 1980.

[13] M.L. Jost, and R.B. Herrmann, "A Students Guide to and Review of Moment Tensors," Seismological Research Letters, vol. 60, no. 2, p. 37-57, Apr. 1989, doi: 10.1785/gssrl.60.2.37.

[14] L. Knopoff, and M.J. Randall, "The compensated linearvector dipole: A possible mechanism for deep earthquakes," Journal of Geophysical Research, vol. 75, no. 26, p. 4957-4963, 1970.

[15] M.N.S. Muqtadir, *et al.*, "Source Analysis of April 2, 2023, Magnitude 5.6 Flores Sea Earthquake North of Bima, Sumbawa, Indonesia," presented at the IOP Conference Series: Earth and Environmental Science, IOP Publishing, 2024, p. 012026.

[16] A. Guilhem Trilla, and Y. Cano, "Using Moment Tensor Inversions for Rapid Seismic Source Detection and Characterization: Application to the North Korean Nuclear Tests," Pure Appl. Geophys., Mar. 2024, doi: 10.1007/s00024-024-03455-7.

[17] J. Hu, T.-S. Phm, and H. Tkali, "Seismic moment tensor inversion with theory errors from 2-D Earth structure: implications for the 20092017 DPRK nuclear blasts," Geophysical Journal International, vol. 235, no. 3, p. 2035-2054, 2023.

[18] A. Caputa, . Rudziski, and S. Cesca, "How to Assess the Moment Tensor Inversion Resolution for Mining Induced Seismicity: A Case Study for the Rudna Mine, Poland," Front. Earth Sci., vol. 9, p. 671207, Jul. 2021, doi: 10.3389/feart.2021.671207.

[19] J. Kan, *et al.*, "Discrimination of microseismic events in coal mine using multifractal method and moment tensor inversion," Fractal and Fractional, vol. 6, no. 7, p. 361, 2022.

[20] C. Liu, *et al.*, "Source types of induced earthquakes in underground mines: Revealed by regional moment tensor inversion," Geomechanics and Geophysics for Geo-Energy and Geo-Resources, vol. 10, no. 1, p. 106, 2024.

[21] F. Rodrguez-Cardozo, *et al.*, "The 20142015 complex collapse of the Brarbunga caldera, Iceland, revealed by seismic moment tensors," Journal of Volcanology and Geothermal Research, vol. 416, p. 107275, 2021.

[22] O. Sandanbata, *et al.*, "Moment tensors of ringfaulting at active volcanoes: Insights into verticalCLVD earthquakes at the Sierra Negra caldera, Galpagos Islands," Journal of Geophysical Research: Solid Earth, vol. 126, no. 6, p. e2021JB021693, 2021.

[23] M. Beyreuther, *et al.*, "ObsPy: A Python toolbox for seismology," Seismological Research Letters, vol. 81, no. 3, p. 530-533, 2010.

[24] J. Havskov, and L. Ottemoller, "Routine data processing in earthquake seismology: with sample data, exercises and software", Springer Science and Business Media, 2010.

[25] M. Wadhawan, D. Hazarika, and S. Saikia, "Recent Developments in Using Seismic Waves as a Probe for Subsurface Investigations: Theory and Practices", Leiden: CRC Press/Balkema, 2022.

[26] S. Stein, and M. Wysession, "An Introduction to Seismology, Earthquakes, and Earth Structure", Blackwell Publishing Ltd., 2003.

[27] R.B. Herrmann, "Computer Programs in Seismology: An Evolving Tool for Instruction and Research," Seismological Research Letters, vol. 84, no. 6, p. 1081-1088, Nov. 2013, doi: 10.1785/0220110096.

[28] D. Dreger, and B. Romanowicz, "Source Characteristics of Event in the San Francisco Bay Region," USGS, Report 94-176, 1994. doi: 10.3133/ofr94176.

[29] A. Chiang, "Time Domain Moment Tensor Inversion in Python," Lawrence Livermore National Laboratory (LLNL),

Livermore, CA (United States), 2020.

[30] A. Chiang, *et al.*, "Source Characterization of Underground Explosions from Combined Regional Moment Tensor and First-Motion Analysis," Bulletin of the Seismological Society of America, vol. 104, no. 4, p. 1587-1600, Aug. 2014, doi: 10.1785/0120130228.

[31] S.I. Franco, A. Iglesias, and E. Fukuyama, "Moment tensor catalog for Mexican earthquakes: almost two decades of seismicity," Geofsica internacional, vol. 59, no. 2, p. 54-80, 2020.

[32] P. Kol, "Kagan Angle" (https://www.mathworks.com/matlabcentral/fileexchange/70040-kagan-angle). (2024). Accessed: Dec. 16, 2024. [Online]. Available: (https://www.mathworks.com/matlabcentral/fileexchange/70040-kagan-angle)

[33] G. Ekstrm, M. Nettles, and A. Dziewoski, "The global CMT project 20042010: Centroid-moment tensors for 13,017 earthquakes," Physics of the Earth and Planetary Interiors, vol. 200, p. 1-9, 2012.

[34] U.S. Geological Survey, "Search Earthquake Catalog." Accessed: Dec. 16, 2024. [Online]. Available: https://earthquake.usgs.gov/earthquakes/search

[35] GEOFON Data Center, "GEOFON Seismic Network." GFZ Data Services, 1993. doi: 10.14470/TR560404.

[36] M.N. Fahmi, *et al.*, "Implementing and evaluating an automatic centroid moment tensor procedure for the Indonesia region and surrounding areas," Earth and Planetary Physics, vol. 8, no. 4, p. 609-620, 2024.

[37] Y. Kagan, "3-D rotation of double-couple earthquake sources," Geophysical Journal International, vol. 106, no. 3, p. 709-716, 1991.

[38] S. Pondrelli, *et al.*, "The Italian CMT dataset from 1977 to the present," Physics of the Earth and Planetary Interiors, vol. 159, no. 3-4, p. 286-303, Dec. 2006, doi: 10.1016/j.pepi.2006.07.008.

[39] J.-Y. Lin, *et al.*, "Crustal thickening and extension induced by the Great SumatraAndaman earthquake of 26 December 2004: revealed by the seismic moment tensor element Mrr," Marine Geophysical Research, vol. 36, p. 187-195, 2015.

[40] M.M. Mukti, *et al.*, "Structural evolution of backthrusting in the Mentawai Fault Zone, offshore Sumatran forearc," Geochemistry, Geophysics, Geosystems, vol. 13, no. 12, 2012.

[41] M. Nakano, *et al.*, "Centroid moment tensor catalogue for Indonesia, Physics of the Earth and Planetary Interiors, vol. 183, no. 3-4, p. 456-467, 2010.

[42] M. Diament, *et al.*, "Mentawai fault zone off Sumatra: A new key to the geodynamics of western Indonesia," Geology, vol. 20, no. 3, p. 259-262, 1992.

[43] D. Tian, *et al.*, "PyGMT: A Python interface for the Generic Mapping Tools". (Dec. 2024). Zenodo. doi: 10.5281/zenodo.14535921.